DANMARKS OG GRØNLANDS GEOLOGISKE UNDERSØGELSE RAPPORT 2001/89

Effective permeability of fracture networks – the 2D penalty

Peter Frykman

GEOLOGICAL SURVEY OF DENMARK AND GREENLAND
MINISTRY OF ENVIRONMENT AND ENERGY

G E U S

DANMARKS OG GRØNLANDS GEOLOGISKE UNDERSØGELSE RAPPORT 2001/89

Effective permeability of fracture networks – the 2D penalty

Peter Frykman

GEOLOGICAL SURVEY OF DENMARK AND GREENLAND
MINISTRY OF ENVIRONMENT AND ENERGY

G E U S

Abstract

A suite of fracture networks with different fracture densities are analysed, and a comparison of the percolation threshold and effective permeability for the 3D model and 2D slices in the model is performed. This comparison shows a marked difference between the two analysis methods, especially for low fracture densities. The study shows that it is not sufficient to use 2D based analysis methods for connectivity and flow properties in fracture models. Only for large fracture densities, the 2D permeability is shown to approach the 3D permeability.

Introduction

The analysis of flow properties of fracture networks has received interest in disciplines such as petroleum engineering, hydrogeology and geothermal applications. The tools for analysing these properties are diverse, ranging from the traditional finite difference tools in reservoir flow simulation, to newer developments of finite element methods. The latter seems best suited for reflecting the transport properties of the discrete elements that fractures can be viewed as, but lack the efficiency and solution power for larger problems. For working with large problems or volumes with many fractures, some simplifications are necessary, and the reduction of the problem to 2D has been tried for developing rules for flow as a function of other geometric parameters (Sarda et al. 1999). Others have tried more analytical ways to extract information about the behaviour of 3D models (Koudina et al. 1998).

For the purpose of testing the relation between 2D and 3D methods, one single type of fracture network have been selected here and analysed for the relation between fracture density and the effective permeability. As the flow in fracture networks is highly depending on the geometric parameters, this case cannot be used for global description of this relation, but is exclusively used for outlining a procedure for analysis and as illustration of the differences that arrive due to the reduction in pathway connectivity when going from 3D to 2D analysis.

Method

The effective permeability of a quasi-realistic three-dimensional network of polygonal fractures is determined by fine gridding of the geometrical description and a calculation of the permeability of the volume by flow simulation. The fractures are described geometrically as 3D irregular polygons and assigned a constant aperture. The transmissibilities between the grid cells are calculated from these fracture apertures and an effective permeability tensor is determined by flow simulation of the volume in the three main directions.

For the analysis of the fracture networks, the following procedure has been utilised:

- Generation of a discrete fracture network (DFN) model in a cube of 20 m sidelength using FracMan[1]. Repeated generation for a number of different fracture densities.
- Transfer of DFN to CMoS[2]. Gridding the cube into regular grid of 40x40x40 cells. For each cell is calculated the cell interface fracture permeability in the x, y, and z direction.
- Up-scaling to an effective fracture permeability for the full cube of 20x20x20 m assuming zero matrix permeability. The up-scaling procedure is based on the solution to the 1-phase steady state flow equation for an incompressible fluid solved on the user specified grid.
- Selection of 20 sections (2D slices) in the 3D model, and up-scaling to an effective permeability for these slices. Calculation of fracture density for the 2D sections.

Input for DFN

The fracture models are produced with FracMan as a 3D model with discrete geometrical description of the individual fractures in the network (Fig. 1). The fractures are generated using a Baecher model, which is a model for generating populations of discrete fractures that are assumed to be planar, elliptical, and located at random (Baecher et al. 1977). The Enhanced Baecher model, is an extension of the Baecher model that provides for termination of fractures at intersections with pre-existing fractures. The model generates polygonal fractures that may or may not terminate at intersections with other fractures.

There are two ways of generating fractures; by randomly generating the fracture center points, or by randomly generating an arbitrary point on the fracture surface. Selection of the Surface Points option eliminates the edge effects at the expense of more computational effort.

The FracMan package idealises fractures as planar and polygonal. The planarity simplification is adopted for three reasons: firstly, because little field data is available on non-planar fractures; secondly, because planar fractures are computationally far more tractable than undulating fractures; and thirdly, because for problems of concern the effects of fracture undulation can be approximated in a more tractable manner, e.g., as an increased coefficient of friction for mechanical problems, or as an adjusted transmissivity for hydrological problems. The assumption of polygonal fractures is both realistic and useful, as it allows the approximate representation of a wide variety of fracture shapes by a single mathematical form. Considerations from fracture mechanics suggest that in homogeneous rock the general shape of an isolated fracture should be elliptical, as is

---

[1] FracMan™ is a software package from Golder Associates used for fracture modelling and analysis (v. 2.603).

[2] CMoS™ is a software package for Chalk Model Synthesis developed by COWI A/S for gridding and upscaling.

assumed in the Baecher model (Baecher et al. 1977). However, since rock is generally heterogeneous, perfectly elliptical fractures are unlikely, and in a practical sense no error is introduced by representing the ideal, elliptical fracture by a many-sided polygon of equivalent area. Moreover, observed fractures are generally polygonal due to terminations of the fractures at intersections with other fractures.

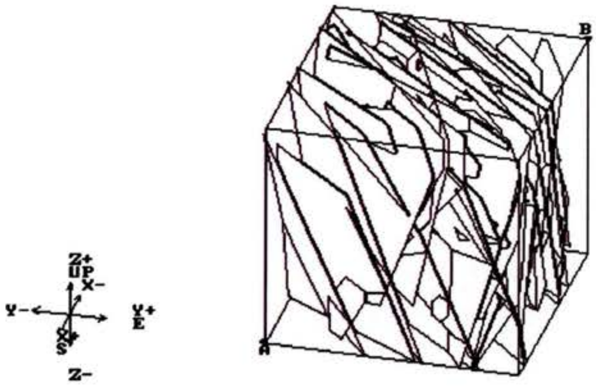

Figure 1

Example of a model 20x20x20 m with 2 fracture sets in a conjugate system with steeply dipping fractures at a 45^o angle. Each set with 0.6 density m^2/m^3 , total density 1.2 m^2/m^3

Directional distribution

The distribution of orientations is shown on Figure 2. The input is specified as a Fisher distribution with dispersion 800, which causes a narrow spread of the fracture orientations. Examples from outcrop investigations in chalk show more scattered distributions (Koestler & Reksten 1995), but the narrow spread is chosen here for simplicity of the DFN.

The univariate Fisher distribution is defined by a probability density function (Mardia 1972) with a distribution parameter k (specified by the user). This distribution is unimodal and symmetric about the center axis. Increasing k produces a distribution more concentrated around the center. Uniform distribution corresponds to k= 0. A value of k between 1 and 5 gives high orientation variability and between 20 and 50 gives low orientation variability.

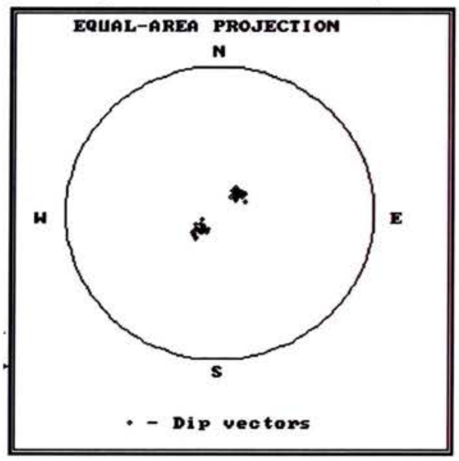

Figure 2

The orientation distribution of dip vectors for a conjugate set with density of 1.2. Each set shows a fairly narrow spread, which might not be fully realistic for natural fracture systems, but is chosen to simplify the geometry of the network.

Size distribution and distribution type

Fracture size is specified in terms of the equivalent radius of the fractures before termination, where the equivalent radius is defined by the radius of the circle with an area equal to the area of the polygon, that represents the fracture. For the fracture model, the fracture size distribution is specified in terms of the mean equivalent radius.

For the size distribution is used a function of Truncated Exponential. The exponential distribution is specified by a probability density function and is completely specified by its mean value x, which in this case has been given as 20 m. The truncated exponential distribution has two additional parameters (x-,x+), the minimum and maximum values, set to 0 and 20 in this case.

Fracture intensity measures

A wide variety of measures are available for quantifying the intensity of geologic features. FracMan allows specification of intensity in terms of the number of fractures in the generation region, Nf, a real intensity, P32, and volume percent, P33. All of these measures are interrelated through the distribution of fracture size (area or volume). They are also related to the more common measure of fracture intensity, and the distribution of spacings between fractures as encountered in a borehole. P32 is defined as the total area of features per unit volume, and should be the preferred intensity measure for fracture intensity, since it is invariant with respect to the distribution of fracture size.

P32 = Af/Vt

where Af is the total area of features and Vt is the total Volume.

P32 is in units of m^2/m^3 = 1/meter or 1/km, but is scale independent (i.e., it does not depend upon the volume studied or the orientation of the measurement). Alternative measures such as the number of features per unit area (P33) is scale dependent, and the P33 is depending on the fracture aperture.

The intensity of faults and fractures are frequently represented in mean spacing, E(Sf), between fractures or faults within a set. The relationship between E(Sf) and P32 depends upon the distribution of the orientation of features relative to the line along which the spacing Sf was measured.

P32 = Cp/E(Sf)

Where Cp = constant dependent upon the distribution of the orientation of features relative to the line along which the spacing Sf was measured. For a uniform distribution of feature organisation, a value of Cp of 2.0 was found (Dershowitz 1984). For most fracture geometries, Cp will vary between 1.0 and 3.0. The exact value of Cp for a particular fracture network and borehole geometry can be found by simulated borehole sampling.

Feature intensity on trace planes can be quantified in terms of the mean feature spacing, the number of features per unit area, or by the measure P21 defined by Dershowitz (1984) as

P21 = Lf/At

where Lf = Total length of feature traces on the two dimensional feature, and At = Total area of the surface, This measure is used, for example, when feature intensity must be derived from lineament maps (Fig. 3). The relationship between P21 and P32 depends upon the relationship between the feature orientation distribution and the orientation of the surface on which P21 was calculated

P32 = C32*P21

where C32 is a proportionality constant related to the orientation distribution of the features. For most fracture geometric patterns, values for C32 vary between 1 and 3 (Dershowitz, 1984). For a uniform distribution of orientations, a value of 1.3 ($4/\pi$) can be used.

Figure 3
Lineament map for a 2D vertical section (20x20 m) in a model with density 8.

Fracture aperture

The estimation of apertures for fractures is both locally highly uncertain due to measurement problems, and also spatially highly variable since aperture must be fluctuating on the fracture planes. The fractures in the present models have all been assigned a constant aperture of 100 microns, which is used throughout the permeability calculation.

For fractures where roughness is assumed, the grid cell intrinsic fracture permeability is calculated from the hydraulic aperture (Ah) and the mechanical aperture (Am), both apertures given in microns.

$K_{frac} = 1013.25\ (Ah^3/12Am)\ (mD)$

In case the mechanical aperture equals the hydraulic aperture (no roughness) the intrinsic fracture permeability formula reduces to the parallel plate formula given an aperture value A:

$$k_{frac} = 1013.5 \cdot \frac{A^2}{12}$$

The hydraulic aperture in microns is given by the mechanical aperture in microns and the Joint Roughness Coefficient (JRC)(Barton 1973; Barton & Bandis 1990).

$$Ah = \frac{Am^2}{JCR^{2.5}}$$

Example calculations:

1. Mechanical aperture = 500 micron, JRC = 20,
   result: Hydraulic aperture = 140 micron (permeability = 461 Darcy)
2. Mechanical aperture = 500 micron, JRC = 15,
   result: Hydraulic aperture = 287 micron (permeability =3884 Darcy)

Permeability calculation and upscaling to effective properties

When the purely geometrical model has been constructed with FracMan, the model is transferred to an analysis tool CMoS™, in which the geometrical description (Fig. 4) can be converted into a grid description of the hydraulic parameters.

The sequence of events in CMoS is:

1. Calculation of the intrinsic fracture permeability (mD) in each cell using the aperture formula: $$k_{frac} = 1013.5 \cdot \frac{A^2}{12}$$
2. Calculation of the Cell Transmissibility Factor FD for each cell interface as the ratio of Fracture-area/Cell-interface-area (i.e. 6 values pr. cell, all between 0.0 and 1.0).
3. Calculation of the Cell Interface Fracture Permeability as the harmonic average of the intrinsic fracture permeabilities in the two adjacent cells multiplied with the FD for that interface (i.e. 6 values pr. cell)
4. Definition of upscaling blocks (= subsections of the volume to be up-scaled).
5. Up-scaling of the block properties by flow simulation (no-flow or periodic boundary conditions can be selected) which gives the permeability tensor for each block.

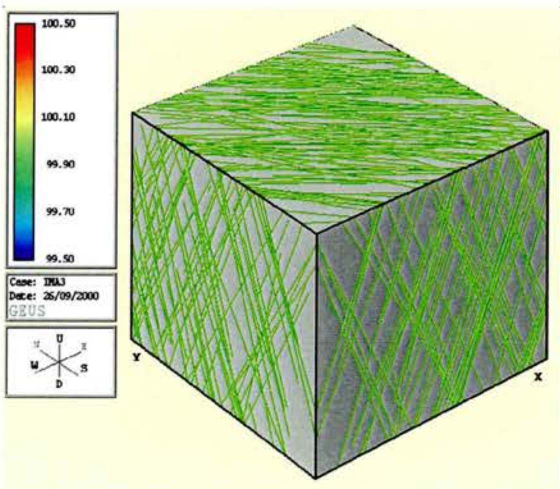

Figure 4

3D view of the density=6 model in CMoS. All fractures have been assigned an aperture of 100 micron.

The present geometrical model has been subdivided into a regular grid of 40x40x40 cells. The grid cell intrinsic fracture permeability k_{frac} in mD is calculated (Fig. 5) from the aperture A given in microns with the parallel plate formula

$$k_{frac} = 1013.5 \cdot \frac{A^2}{12}$$

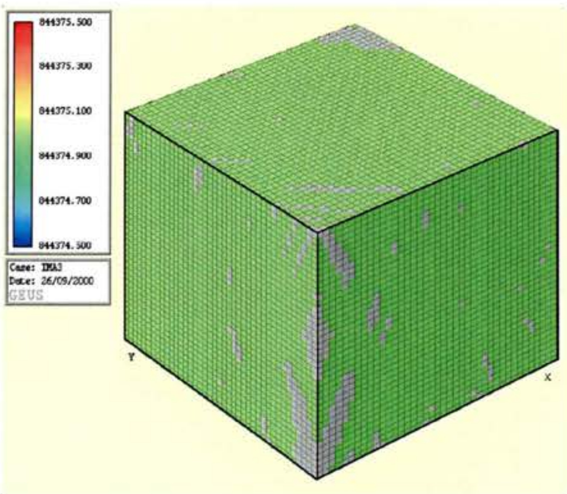

Figure 5

The gridding of the model shows that most cells contain a fracture that has a constant intrinsic permeability of 844 Darcy.

In order to describe connectivity between neighbouring cells, the transmissibility values are calculated for all 6 sides as the ratio between the fracture-area/cell-interface-area (Fig. 6). These values are then used during the upscaling as input for the flow simulation that determines the effective permeability for the model.

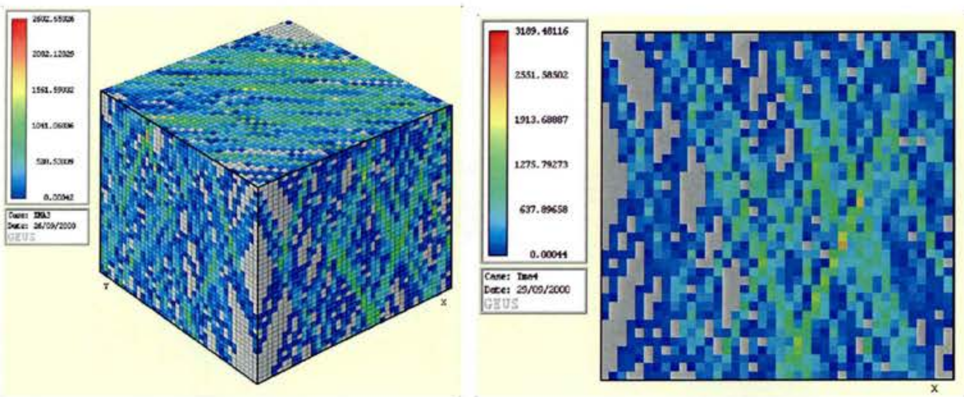

Figure 6

The description is gridded with a regular grid and the transmissibility factor for each cell is calculated from the aperture, number of fractures in each cell and cell interface area.

The gridded model is then upscaled to an effective permeability tensor for the full model volume. The up-scaling procedure is based on the solution to the 1-phase steady state flow equation for an incompressible fluid. The flow calculations are performed with periodic boundary conditions in order to capture the cross-flow effects, which is seen to be significant due to the main orientation of the fractures in a 45° pattern (Fig. 7). However, the differences between the no-flow and periodic boundary calculations are small as long as there exists a connected path between the two sides in the main directions (Fig. 8).

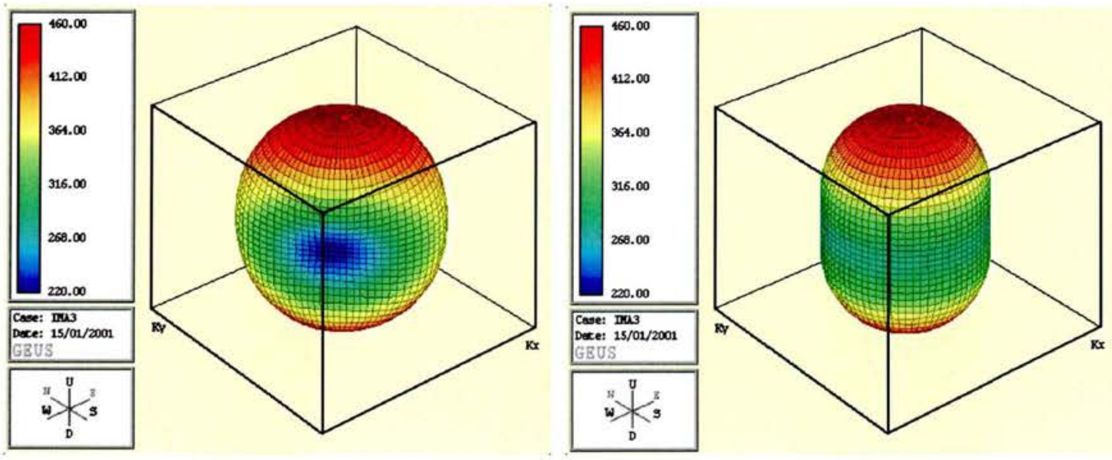

Figure 7
Up-scaled permeability for the full volume.
A: Calculated with periodic boundaries; B: Calculated with no-flow boundary conditions. The permeability in a certain direction is the length from origo (centre of box) to the surface.

Comparison of the main-axis permeabilities shows the similarity between the two methods (Table 1), but for the calculation with periodic boundary conditions the cross-flow terms are significant, and the calculated tensor main-direction conforms with the fracture pattern direction of 45°.

Table 1. Boundary conditions for simulation	Kxx mD	Kyy mD	Kzz mD	Kxy, Kyx	Kxz, Kzx	Kyz, Kzy	Angle
Periodic	291	295	463	-67.4	-32.5	-16.7	-44°
No-flow	283	288	460				

In a further upscaling perspective, the calculations with periodic boundary conditions indicate that if the upscaled block is re-used for a larger model and is inserted in a larger grid, the cross-flow term is traditionally not represented in the flow calculation at this larger step. The problem of this missing contribution can either be solved by implementing the tensor description in the flow simulator used at the larger scale, or by re-orienting the grid for the larger scale flow simulation so it conforms with the main flow direction. The last solution requires that there is some uniformity in the main flow direction in the larger scale model.

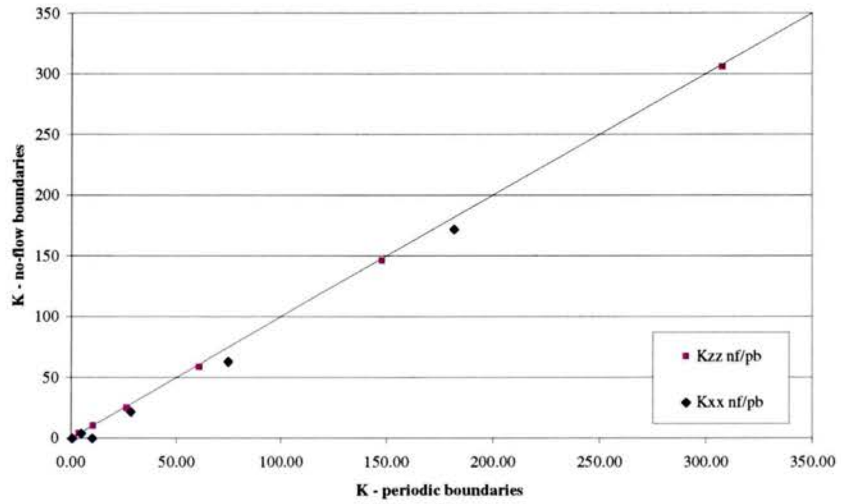

Figure 8

Comparison of the effective permeabilities for 3D volumes calculated with periodic boundaries and no-flow boundaries respectively for a series of models with different fracture densities. The difference between the two methods is not significant as long as there is a connected path between the two sides in the main direction.

After deriving the permeability tensor for the 3D volume, a comparison to the effective permeability for 2D slices in the same model is carried out. For this purpose, 20 sections are extracted in the East-West direction (Fig. 9). For the calculation of effective permeability of the 2D slices, no-flow boundary conditions have been used in order to exclude the 2D cross-flow effect.

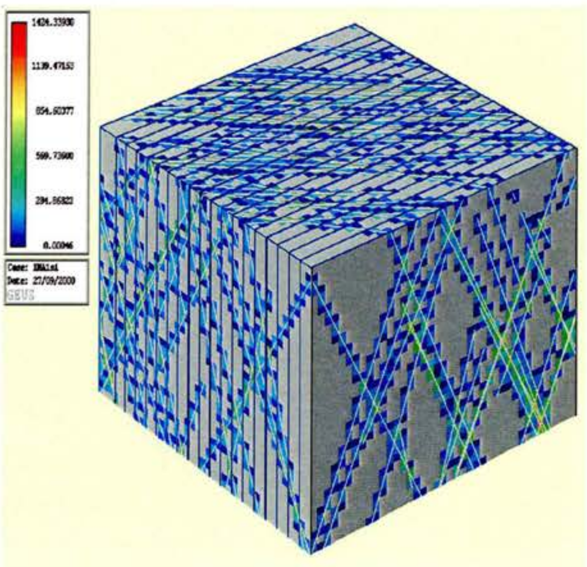

Figure 9

Illustration of the position of the 20 slices (2D) extracted from the 3D model for the subsequent 2D-network analysis. Each slice is physically 0.02 m thick, and is spaced approximately at 1 m through the model. A model with lower fracture density than that previously illustrated is chosen for this illustration.

When comparing the 3D and 2D results it is seen that the 2D permeability values consistently falls below the 3D permeability for the same model (Fig. 10).

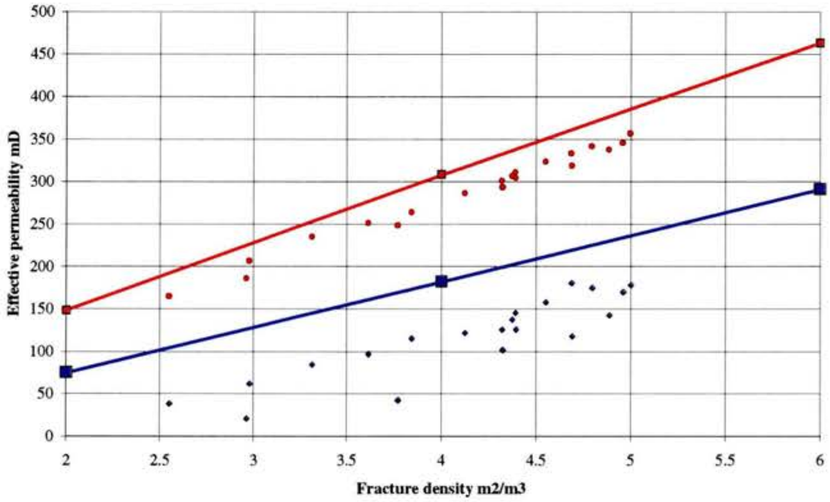

Figure 10

Plot of density=4 permeability data. The upper data set (red line) is the Kz (the vertical permeability component) measured for the 3D volume, and associated points (red) are for the 20 slices containing a 2D model through the 3D model. The lower data set (blue line for 3D and points for 2D) is for the Kx direction.

Discussion

The systematic trend for the decrease in permeability as the fracture density is decreased (Fig. 11) has also been seen in other studies, and the shape of the 3D decline is similar to another 3D study as shown in Figures 12 and 13 (Koudina et al. 1998).
For high fracture densities the 2d permeability approach the 3D value. For lower densities there is a separation between the two measures due to the missing dimension and the loss of associated connectivity in the 2D models. In the density range of 0.1-0.4 an abrupt decrease to zero in 2D permeability occurs. This jump occurs in an interval where the 3D permeabilities follow the regular curve as shown in other studies.
The explanation for this jump is interpreted as caused by the loss of a continuos fracture connectivity across the 2D model in combination with the method of no-flow boundary conditions in the upscaling procedure, and as such indicates the percolation threshold.

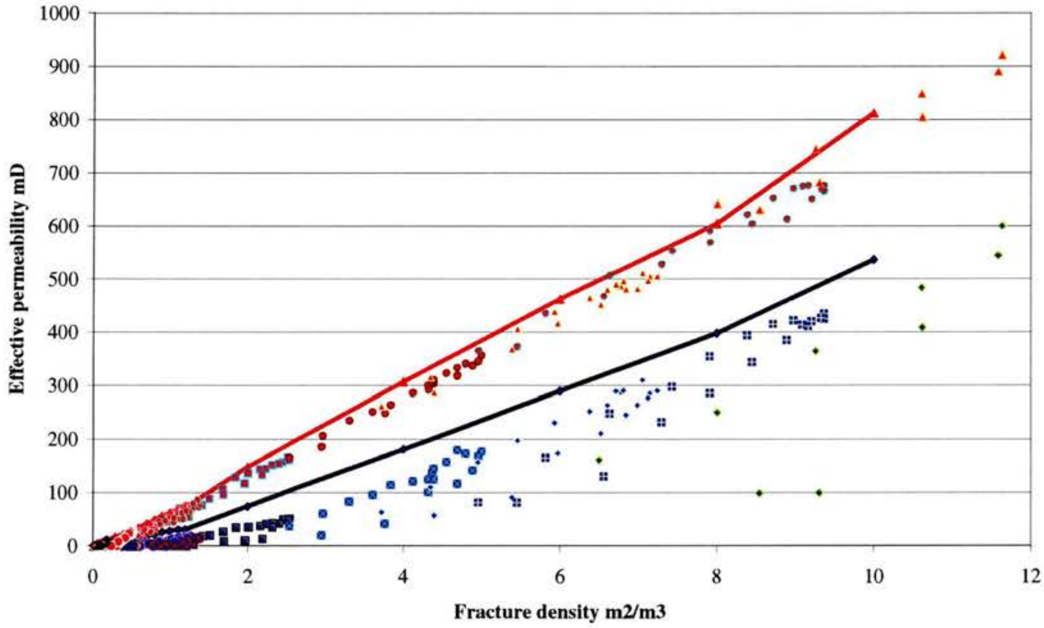

Figure 11
Relation between fracture density and the effective permeability (linear scales). The 3D analysis is shown with line connecting data points, the 2D data is shown as separated points. The upper data set in red colour is for the Kz permeability (vertical), the lower in blue colours is for the Kx direction. For high fracture densities it is seen that the 2D permeability approaches the 3D permeability.

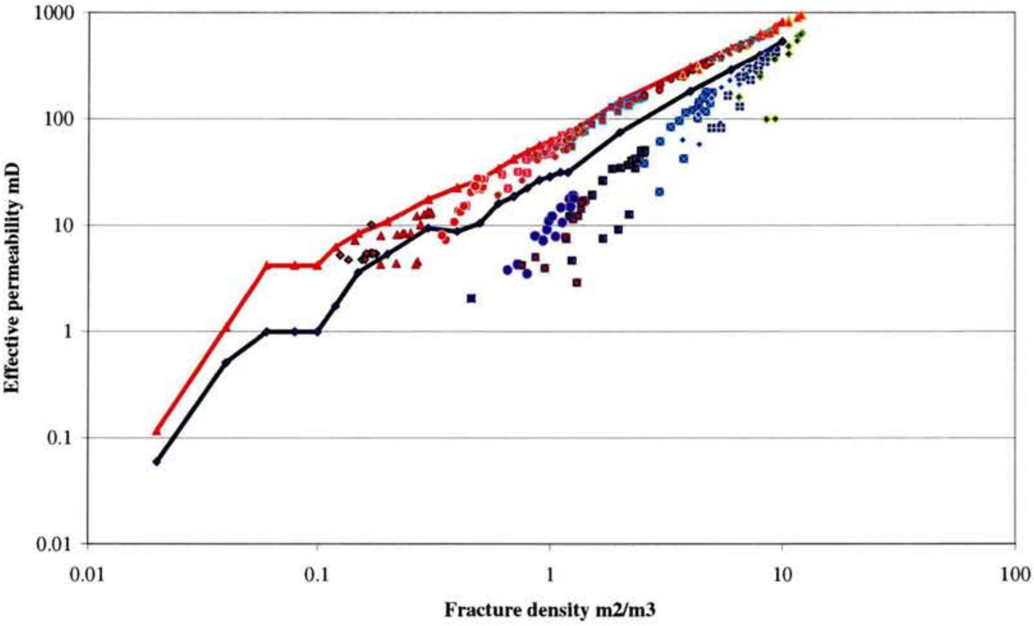

Figure 12

Relation between fracture density and the effective permeability (log-log plot). The 3D analysis is shown with line connecting data points, the 2D data is shown as separated points. The upper data set in red colour is for the Kz permeability (vertical), the lower in blue colours is for the Kx direction. It is seen that the Kx for the 2D models goes to zero around the density of 0.4, while Kz goes to zero around 0.1 due to the more extensive vertical continuity of the few remaining fractures at the low densities.

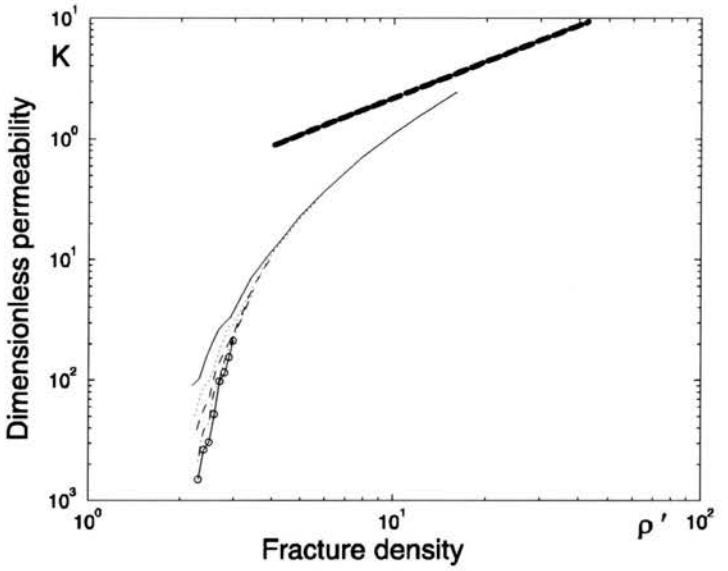

Figure 13

Dimensionless permeability K of networks of monodisperse regular hexagonal fractures as a function of the density (log-log plot). The heavy broken line is for the equation derived for isotropic networks of regular fractures (Snow 1969), which overestimates the permeabilities for most densities analysed. Figure reproduced from (Koudina et al. 1998).

Conclusion

The comparison of effective permeability analyses for 3D and 2D representations of a fracture network shows that the calculated 2D permeabilities are consistently lower than the 3D permeability. The exact relation is depending on the specific case studied. The 2D-permeability trend also shows a clear percolation threshold that is at a much higher fracture density than in a 3D model. These differences arise due to the difference in connectivity depending on if a 3D or a 2D model is treated. The difference constitute the penalty that is introduced if a fracture model is investigated in 2D and not in 3D, and is a warning that tools capable of performing 3D analyses should always be used to avoid these negative effects. The two tools used for fracture modelling and for gridding and upscaling are found to be efficient for this type of 3D analysis.

References

Baecher, G.B., Lanney, N.A. & Einstein, H.H. 1977: Statistical Description of Rock Properties and Sampling. 18th U.S. Symposium on Rock Mechanics, American Institute of Mining Engineers, 5C, 1-8, .

Barton, N. 1973: Review of a new shear-strength criterion for rock joints. Engineering Geology 7, 287-332.

Barton, N. & Bandis, S. 1990: Review of predictive capabilities of JRC-JCS model in engineering practice. In: Barton, N. & Stephansson, O. (eds): Rock Joints, 603-610. Rotterdam: Balkema

Dershowitz, W.S. 1984: Rock Joint Systems. Unpublished Ph.D. thesis, Massachusetts Institute of Technology, Cambridge, MA.

Koestler, A.G. & Reksten, K. 1995: Fracture-network 3D characterization in a deformed chalk reservoir analogue - the Lägerdorf case. SPE Formation Evaluation 10(3), 148-152 (also SPE 28728).

Koudina, N., Garcia, R.G., Thovert, J.F. & Adler, P.M. 1998: Permeability of three-dimensional fracture networks. Physical Review E 57(4), 4466-4479.

Mardia, K.V. 1972: Statistics of Directional Data. New York, NY: Academic Press.

Sarda, S., Bourbiaux, B. & Cacas, M.C. 1999: Correlations between natural fracture attributes and equivalent dual-porosity model. EAGE - 10th European Symposium on Improved Oil Recovery, Brighton, UK, 18-20 August 1999, 11.

Snow, D.T. 1969: Anisotropic permeability of fractured media. Water Ressources Research 5, 1273-1289.